Failure mechanisms in coupled poro-plastic medium

Emina Hadzalic, Adnan Ibrahimbegovic, Mijo Nikolic

Coupled Systems Mechanics, *Vol. 7, No. 1 (2018) 43-59*
DOI: https://doi.org/10.12989/csm.2018.7.1.043

Failure mechanisms in coupled poro-plastic medium

Emina Hadzalic[1,2a], Adnan Ibrahimbegovic[*1] and Mijo Nikolic[1,3b]

[1]*Université de Technologie de Compiègne/Sorbonne Universités, Laboratoire Roberval de Mécanique, Centre de Recherche Royallieu, 60200 Compiègne, France*
[2]*Faculty of Civil Engineering, University of Sarajevo, Patriotske lige 30, Sarajevo 71000, Bosnia and Herzegovina*
[3]*Faculty of Civil Engineering, Arhitecture and Geodesy, University of Split, Matice Hrvatske 15, 21000 Split, Croatia*

(Received March 25, 2017, Revised April 1, 2017, Accepted April 3, 2017)

Abstract. The presence of the pore fluid strongly influences the reponse of the soil subjected to external loading and in many cases increases the risk of final failure. In this paper, we propose the use of a discrete beam lattice model with the aim to investigate the coupling effects of the solid and fluid phase on the response and failure mechanisms in the saturated soil. The discrete cohesive link lattice model used in this paper, is based on inelastic Timoshenko beam finite elements with enhanced kinematics in axial and transverse direction. The coupling equations for the soil-pore fluid interaction are derived from Terzaghi's principle of effective stresses, Biot's porous media theory and Darcy's law for fluid flow through porous media. The application of the model in soil mechanics is illustrated through several numerical simulations.

Keywords: discrete beam soil; discrete beam lattice model; poroplasticity; coupling; failure mechanisms

1. Introduction

The fundamental principle in soil mechanics that has a crucial role in understanding and modeling the behavior of soil is Terzaghi's principle of effective stresses. According to this principle, the total normal stress is equal to the sum of the effective stress and the pore pressure. The effective stress represents the part of the total stress carried by the soil skeleton, and the pore pressure represents the part of the total stress carried by the water in the pores. All changes in the soil related to the strength or deformability are due to changes in effective stress, e.g., consolidation or shear resistance. In general, the presence of water in soil can increase the risk of final failure. For example, heavy rain can trigger landslide in the slope that was once stable due to the reduction in the shear strength of the soil. To be able to better understand and predict failure

*Corresponding author, Chair for Computational Mechanics, Professor,
E-mail: adnan.ibrahimbegovic@utc.fr
[a]Ph.D., E-mail: emina.hadzalic@utc.fr or emina.hadzalic@gf.unsa.ba
[b]Postdoctoral researcher, E-mail: mijo.nikolic@gradst.hr

http://www.techno-press.org/?journal=csm&subpage=8 ISSN: 2234-2184 (Print), 2234-2192 (Online)

phenomena in the soil, interaction between soil and pore fluid has to be taken into account.

The pioneering works in soil-pore fluid interaction are Terzaghi's theory of one-dimensional consolidation (Terzaghi 1943), and Biot's theory of three-dimensional consolidation (Biot 1941). Both theories are limited to the case of linear elastic behavior of the soil. This is a reasonable assumption if the settlement of the soil subjected to external loading is to be calculated (Singh and Sawant 2014). Biot's porous media theory is further extended to take into account nonlinearities of the soil in the pre-peak part of the response (Prevost 1983, Zienkiewicz and Shiomi 1984, Lewis and Schrefler 1998).

Biot's coupled theory has been extensively used as one of the ingredients in the finite element analysis of localized failure and influence of the fluid flow through the discontinuities on the response of the porous medium. Finite element simulation based on the concept of regularized discontinuity has been used to model localization and progressive development of shear bands in an elastoplastic porous medium (Larsson and Larsson 2000). Finite element method based on the partition-of-unity property of finite element shape functions has been used to model the propagation of discontinuities in fluid saturated medium, and to model the fluid flow through the fracturing unsaturated porous medium (Borst *et al*. 2006, Réthoré *et al*. 2008, Secchi and Schrefler 2014). Localized failure based on embedded strong discontinuity formulation is analysed in (Armero and Callari 1999, Callari and Armero 2002, 2004) for a saturated poro-plastic medium, and in (Callari *et al*. 2010) for a partially saturated medium. Beside continuum models, discrete lattice models have also been used for modeling coupled solid-fluid problems. The discrete beam lattice model proposed in (Nikolic and Ibrahimbegovic 2016) with cohesive links based on Timoshenko beam finite elements with embedded strong discontinuities in axial and transverse direction has been used to predict localized failure in fluid saturated rock materials. The coupling between the solid and the fluid phase is governed by Biot's theory. In the proposed model, fluid flow takes place through the same mesh of Timoshenko beam finite elements used to obtain the mechanical response. Discrete lattice models in which the fluid flow and mechanical response are obtained on the same network of lattices have also been used in modeling one-way coupling problems of chloride diffusion in cracked concrete (Šavija *et al*. 2013, 2014), and to simulate cracking in concrete due to shrinkage (Bolander and Berton 2004). A discrete lattice model in which the fluid flow is spread through the dual lattice network is used to model the influence of cracking on the fluid flow in concrete (Grassl 2009).

In this paper, we extend the use of the model proposed in (Nikolic and Ibrahimbegovic 2016) to the problems encountered in soil mechanics. Our goal is to investigate the coupling effects and to capture failure mechanisms in the soil (Hadzalic et al. 2017), which are fully saturated with fluid and subjected to external loading. We also analyze the time evolution of the excess pore pressures in the situations when the soil exhibits dilatant and contractive behavior.

The outline of the paper is as follows. In Section 2, we provide a brief description and finite element formulation of the plain strain discrete beam lattice model used in the failure analysis of the poro-plastic medium. In Section 3, we present the results obtained on the set of numerical examples: plain-strain linear elastic consolidation analysis, plain strain compression test and coupled soil-foundation system. In section 4, we give concluding remarks.

2. Discrete beam lattice model for the analysis of poro-plastic medium

The main idea behind the uncoupled discrete beam lattice model is that the structure of the soil sample can be represented as an assembly of Voronoi cells. Voronoi cells represent parts of the

material that are held together with cohesive links. The macroscale response of soil is thus obtained on the model in which the domain is meshed with one-dimensional elements acting as cohesive links. The meshing of the domain and computation of the cross-sectional properties of one-dimensional finite elements is done in a very efficient manner by exploiting the property that the Voronoi diagram is dual to Delaunay triangulation. Namely, the end result of Delaunay triangulation preformed on the given domain is a mesh of triangles. The mesh of one-dimensional finite elements is then obtained by positioning the finite elements along the edge of every triangle. The duality property enables the computation of a Voronoi diagram from the set of points that correspond to the vertices of Delaunay triangles. Every finite element connects two neighbouring Voronoi cells and is perpendicular to the edge shared between those two cells. The area of the finite element is then calculated from the length of that shared edge. The discrete beam lattice model with cross sectional properties of finite elements computed in such manner can successfully reproduce the linear elastic response of an equivalent continuum model as shown in (Ibrahimbegovic and Delaplace 2003, Nikolic *et al*. 2015).

The computed macroscale response and failure mechanisms in soil depend on the type of the finite element used to model the behavior of cohesive links. The discrete beam lattice model with truss bar elements as cohesive links has been previously used for modeling fracturing in concrete (Benkemoun *et al*. 2010, 2012). Truss bar elements with embedded discontinuity in axial direction were able to represent crack formation in mode I that relates to crack opening. To be able to more accurately represent crack propagation and crack coalescence in materials such as rock, concrete or soil, a finite element used for modeling the cohesive link has to be capable of representing both mode I and mode II failure modes. Again, mode I relates to crack creation and mode II relates to crack sliding. For this reason, Timoshenko beam finite elements in (Nikolic *et al*. 2015) provide the embedded discontinuity in both axial and transverse direction. The discrete beam lattice model with Timoshenko beam finite elements acting as cohesive links has been successfully used in modeling behavior and and failure in rocks, both in 2D and 3D setting (Nikolic *et al*. 2015, Nikolic and Ibrahimbegovic 2015).

The discrete beam lattice model proposed in (Nikolic *et al*. 2015) has been extended to take into account the effects of the fluid presence on the failure in rocks (Nikolic and Ibrahimbegovic 2016). In the proposed discrete model, the coupling between the solid and pore fluid is introduced through Biot's porous media theory (Biot 1941) and Darcy's law governing the fluid flow. The fluid flow is spread across the domain through the same network of Timoshenko beam finite elements used for simulating mechanical response. We further extend the use of the proposed model to failure analysis in saturated soils.

2.1 Finite element formulation

In this section we give a short overview of equations governing the soil-pore fluid interaction and finite element formulation of the coupled problem in one-dimensional setting. More details on soil-pore fluid interaction can be found in (Smith and Griffiths 2004, Zienkiewicz and Taylor 2005, Callari and Armero 2004, Nikolic and Ibrahimbegovic 2016). More details on the finite element formulation of inelastic Timoshenko beam finite elements with enhanced kinematics in axial and transverse direction can be found in (Ibrahimbegovic 2009, Nikolic *et al*. 2015, Do *et al*. 2015, Imamovic *et al*. 2015, Nikolic *et al*. 2017). Because the problem of soil-pore fluid interaction is in the class of the first order transient problems, to obtain the solution we will use the method of separation of variables. Here, the space discretization of the solution in terms of nodal

displacements and pore pressures is preformed with the finite element method using standard interpolation functions. The variation of the solution in time is introduced through the time-dependent nodal values of displacements and pore pressures. The solution of the coupled problem is obtained at discrete time points t_0, t_1, ..., t_n using backward Euler scheme.

2.1.1 Kinematics

Consider a straight, two-noded Timoshenko beam finite element of length L^e, and cross section A^e. The element has four degrees of freedom per each node: axial displacement, transverse displacement, rotation of cross section, and pore pressure (Fig. 1). The Timoshenko beam finite element is enhanced with additional kinematics in terms of strong discontinuities introduced in axial and transverse direction. These additional kinematics enable representation of crack formation in modes I and II. Interpolation of enhanced displacement fields and pore pressure is written as

$$u(x,t)=\mathbf{N}\mathbf{u}+M(x)\alpha_u,\ v(x,t)=\mathbf{N}\mathbf{v}+M(x)\alpha_v,\ \theta(x,t)=\mathbf{N}\boldsymbol{\theta},\ p(x,t)=\mathbf{N}^p\mathbf{p} \tag{1}$$

where α_u and α_v are displacements jumps, and

$$\begin{aligned}&\mathbf{u}(t)=\{u_1,u_2\}^T, \quad \mathbf{v}(t)=\{v_1,v_2\}^T\\ &\boldsymbol{\theta}(t)=\{\theta_1,\theta_2\}^T, \quad \mathbf{p}(t)=\{p_1,p_2\}^T\end{aligned},\ \mathbf{N}(x)=\mathbf{N}_{\mathbf{p}}(x)=\{N_1,N_2\}=\left\{1-\frac{x}{L^e},\frac{x}{L^e}\right\} \tag{2}$$

$$M(x)=\begin{cases}-N_2(x), & x\in[0,\bar{x}]\\ H_{\bar{x}}-N_2(x), & x\in[\bar{x},\,1]\end{cases},\ H_{\bar{x}}=\begin{cases}0, & x\le\bar{x}\\ 1, & x>\bar{x}\end{cases} \tag{3}$$

The space derivatives of the displacements fields and the pore pressure, i.e. the strains and pore pressure gradient, are written as

$$\varepsilon(x,t)=\mathbf{B}\mathbf{u}+G(x)\alpha_u,\ \gamma(x,t)=\mathbf{B}\mathbf{v}-\mathbf{N}\boldsymbol{\theta}+G(x)\alpha_v,\ k(x,t)=\mathbf{B}\boldsymbol{\theta},\ \frac{\partial p}{\partial x}(x,t)=\mathbf{B}_p\mathbf{p} \tag{4}$$

where

$$\mathbf{B}=\mathbf{B}_p=\left\{\frac{dN_1}{dx},\frac{dN_2}{dx}\right\}=\left\{-\frac{1}{L^e},\frac{1}{L^e}\right\} \tag{5}$$

$$G(x)=\frac{dM(x)}{dx}=\begin{cases}-\dfrac{1}{L^e}, & x\in[0,\bar{x})\cup(\bar{x},L^e]\\ -\dfrac{1}{L^e}+\delta_{\bar{x}}, & x=\bar{x}\end{cases} \tag{6}$$

where $\delta_{\bar{x}}$ is the Dirac function

$$\delta_{\bar{x}}=\begin{cases}0, & x\in[0,\bar{x})\cup(\bar{x},L^e]\\ \infty, & x=\bar{x}\end{cases} \tag{7}$$

The time derivatives of the displacement fields and pore pressure are written as

$$\frac{\partial u}{\partial t}(x,t)=\mathbf{N}\dot{\mathbf{u}},\ \frac{\partial v}{\partial t}(x,t)=\mathbf{N}\dot{\mathbf{v}},\ \frac{\partial \theta}{\partial t}(x,t)=\mathbf{N}\dot{\boldsymbol{\theta}},\ \frac{\partial p}{\partial t}(x,t)=\mathbf{N}^p\dot{\mathbf{p}} \tag{8}$$

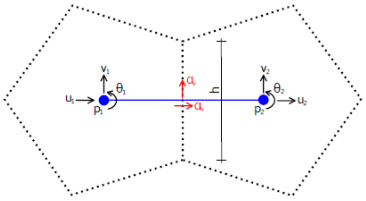

Fig. 1 Timoshenko beam finite element with enhanced kinematics

2.1.2 Constitutive equations

The pre-peak response of the Timoshenko beam finite element is described with the classical elastoplastic model. The elastic part of the model is represented with Hooke's law, and the plastic part with plasticity with linear isotropic hardening. The post-peak response of the element is described with exponential softening. The behavior of the element in bending is purely linear elastic.

Plasticity with linear isotropic hardening. The full set of equations for the plasticity model with linear isotropic hardening is derived using thermodynamics and the principle of maximum plastic dissipation (Ibrahimbegovic 2009). The model is characterized with additive decomposition of the total deformation ε into elastic ε^e and plastic part ε^p, with only the elastic part influencing the value of the stresses

$$\varepsilon = \varepsilon^e + \varepsilon^p \tag{9}$$

The strain energy function is defined in terms of strains ε and internal variables, plastic deformation ε^p and strain-like hardening variable ξ

$$\psi\left(\varepsilon, \varepsilon^p, \xi\right) = \frac{1}{2}\left(\varepsilon - \varepsilon^p\right) C \left(\varepsilon - \varepsilon^p\right) + \frac{1}{2} \xi K \xi \tag{10}$$

where C is the is the elastic constant (E or G), and K the hardening modulus.

The plasticity criterion is given in terms of stresses σ and the dual variable $q=K\xi$

$$\phi(\sigma, q) = |\sigma| - \left(\sigma_y - q\right) \le 0 \tag{11}$$

The evolution equations for internal variables ε^p, and ξ, along with the loading/unloading conditions are obtained through the principle of maximum plastic dissipation and Kuhn-Tucker optimality condition

$$\frac{\partial \varepsilon^p}{\partial t} = \frac{\partial \overline{\gamma}}{\partial t} sign(\sigma), \ \frac{\partial \xi}{\partial t} = \frac{\partial \overline{\gamma}}{\partial t} \tag{12}$$

$$\frac{\partial \overline{\gamma}}{\partial t} \ge 0, \ \phi \le 0, \ \frac{\partial \overline{\gamma}}{\partial t} \phi = 0 \tag{13}$$

where $\overline{\gamma}$ is the plastic multiplier.

The value of the plastic multiplier is obtained from the consistency condition

$$\frac{\partial \overline{\gamma}}{\partial t} \frac{\partial \phi}{\partial t} = 0 \tag{14}$$

Exponential softening. Once the element enters the softening phase, the jump in displacement is activated. All plastic deformation from that point on remains localized at the discontinuity whereas the bulk part of the element unloads elastically. The yield function which defines if the

element has entered the softening phase is defined at the discontinuity and is written in terms of stresses σ and dual variable $\bar{\bar{q}}$

$$\bar{\bar{\phi}}\left(\mathrm{t},\bar{\bar{q}}\right)=|\sigma|-\left(\sigma_u-\bar{\bar{q}}\right)\le 0 \tag{15}$$

where t is the internal force acting at the discontinuity, and $\bar{\bar{q}}$ is the stress-like softening variable that for exponential softening takes following form

$$\bar{\bar{q}}=\sigma_u\left(1-exp\left(-\bar{\bar{\xi}}\frac{\sigma_u}{G_f}\right)\right) \tag{16}$$

where G_f is the fracture energy, and $\bar{\bar{\xi}}$ is the strain-like softening variable.

The evolution equations for internal variables α and $\bar{\bar{\xi}}$ along with the loading/unloading conditions are obtained through the principle of maximum plastic dissipation and Kuhn-Tucker optimality condition

$$\frac{\partial\alpha}{\partial t}=\frac{\partial\bar{\bar{\gamma}}}{\partial t}sign\left(\mathrm{t}\right),\ \frac{\partial\bar{\bar{\xi}}}{\partial t}=\frac{\partial\bar{\bar{\gamma}}}{\partial t} \tag{17}$$

$$\frac{\partial\bar{\bar{\gamma}}}{\partial t}\ge 0,\ \bar{\bar{\phi}}\le 0,\ \frac{\partial\bar{\bar{\gamma}}}{\partial t}\bar{\bar{\phi}}=0 \tag{18}$$

where $\bar{\bar{\gamma}}$ is the plastic multiplier.

The value of the plastic multiplier is obtained from the consistency condition

$$\frac{\partial\bar{\bar{\gamma}}}{\partial t}\frac{\partial\bar{\bar{\phi}}}{\partial t}=0 \tag{19}$$

2.1.3 Soil-pore fluid interaction problem. Equilibrium and continuity condition

Terzaghi's principle of effective stresses states that the total nominal stress is equal to the sum of the effective stress σ' (positive in tension) and pore pressure p (positive in compression)

$$\sigma=\sigma'-bp \tag{20}$$

where b is the Biot coefficient.

This principle is exploited in the formulation of Biot's coupled problem that is based on the equilibrium condition imposed on a porous body and the continuity condition imposed on the fluid flow through that porous body. In the discrete beam lattice model used in this paper, a porous body is Timoshenko beam finite element and the fluid flow through this element occurs in axial direction. The strong from of equilibrium equations for Timoshenko's beam is written as

$$\frac{dN}{dx}+n\left(x\right)=0,\ \frac{dT}{dx}+q\left(x\right)=0,\ \frac{dM}{dx}+T\left(x\right)+m\left(x\right)=0 \tag{21}$$

where $N=N'-bpA,\ T=T',\ M=\mathrm{M}'$. The values of N', T' and M' are calculated from the constitutive equations.

The continuity equation for one-dimensional fluid flow is written as

$$\frac{\partial \zeta}{\partial t} + \frac{\partial q_x}{\partial x} = 0 \tag{22}$$

where ζ is the variation of fluid content, and q_x is the volume of the fluid flowing per second through the unit area of the porous material perpendicular to the x-axis. The variation of fluid content ζ is written as

$$\zeta = \frac{1}{M} p + b \frac{\partial u}{\partial x} \tag{23}$$

where M is Biot modulus.

According to Darcy's law, the rate flow q_x is equal t

$$q_x = -\frac{\kappa}{\mu} \frac{\partial p}{\partial x} \tag{24}$$

where κ is the intrinsic permeability of the medium, and μ is the viscosity of the fluid. The previous equations can also be written as

$$q_x = -\frac{k_x}{\gamma_f} \frac{\partial p}{\partial x} \tag{25}$$

where k_x is the coefficient of the permeability of the medium, and γ_f is the unit weight of the fluid.

By inserting Eqs. (23) and (25) into Eq. (22), a new form of the continuity equation is obtained

$$\frac{1}{M} \frac{\partial p}{\partial t} + b \frac{\partial}{\partial t} \left(\frac{\partial u}{\partial x} \right) - \frac{k_x}{\gamma_f} \frac{\partial^2 p}{\partial x^2} = 0 \tag{26}$$

Two basic assumptions in soil mechanics are that soil particles and the water in the pores are incompressible. Based on these assumptions, the value of Biot coefficient and Biot modulus are commonly taken as $b = 1$ and $M \to \infty$.

Standard Galerkin procedure and finite element discretization preformed on the equilibrium equation (Eq. (21)) and the continuity equation (Eq. (26)) result in two equations of the coupled problem

$$\begin{aligned} \hat{\mathbf{K}}^e \mathbf{d} - \mathbf{Q}^e \mathbf{p} &= \mathbf{f} \\ \mathbf{Q}^{e,T} \dot{\mathbf{d}} + \mathbf{S}^e \dot{\mathbf{p}} + \mathbf{H}^e \mathbf{p} &= \mathbf{q} \end{aligned} \tag{27}$$

where

$$\mathbf{d} = \{u_1, v_1, \theta_1, u_2, v_2, \theta_2\}^T, \ \mathbf{p} = \{p_1, p_2\}^T \tag{28}$$

In Eq. (27), $\hat{\mathbf{K}}^e$ is the statically condensed stiffness matrix, $\mathbf{Q}^e$ is the coupling matrix, and $\mathbf{H}^e$ is the permeability matrix.

$$\mathbf{Q}^e = \int_0^{L^e} \mathbf{B}^T b \mathbf{N}_p \, dx \tag{29}$$

$$\mathbf{S}^e = \int_0^{L^e} \mathbf{N}_p^T \frac{1}{M} \mathbf{N}_p \, dx \tag{30}$$

$$\mathbf{H}^e = \int_0^{L^e} \mathbf{B}_p^T \frac{k_x}{\gamma_f} \mathbf{B}_p dx \tag{31}$$

The stiffness matrix of an element is written as

$$\mathbf{K}^e = \int_0^{L^e} \mathbf{B}^T \mathbf{C} \mathbf{B} dx \tag{32}$$

where C is the elastoplatic tangent matrix. Due to the presence of strong discontinuities in displacement fields, the final product of the finite element discretization of the equilibrim equation is a set of two algebraic equations. The first set considers the equilibrium in the bulk part of the material, and the second set considers the equilibrium at the discontinuity. The values of the displacement jumps are calculated from the condition that the residual at discontinuity equals zero. This enables us to carry out the static condensation. The end result of the condensation process is a statically condensed stiffness matrix with the size that corresponds to the size of the nodal displacements vector. For a clearer presentation of results for soil-pore fluid interaction, the process of static condensation will not be elaborated further; for details see (Ibrahimbegovic 2009, Nikolic *et al*. 2015).

3. Numerical simulations

In this section we present the results of selected numerical simulations, which can illustrate an excellent model performance. All numerical computations are performed with the research version of the computer code FEAP, developed by R.L. Taylor (Zienkiewicz and Taylor 2005). In each example, the mesh is generated by using Delaunay triangulation and GMSH software (Geuzine and Remacle 2009).

3.1 Plain strain consolidation analysis

In this section we preform a plain strain consolidation analysis of a Biot poro-elastic solid (Smith and Griffiths 2004). The configuration of the problem is shown in Fig. 2(a). The sample fully saturated with water is subjected to the ramp loading shown in Fig. 2(b). The mechanical properties of the Timoshenko beam finite element used in the computation are shown in Table 1. We assume that soil particles and water are incompressible, hence $b=1$ and $M^{-1}=0$.

Table 1 Mechanical properties of the Timoshenko beam finite element

Young's modulus (kPa)	Poisson's ratio	Coefficient of permeability (m/s)	Unit weight of water (kN/m^3)
$E=1.0$	$v=0.0$	$k=1.0$	$\gamma_f = 1.0$

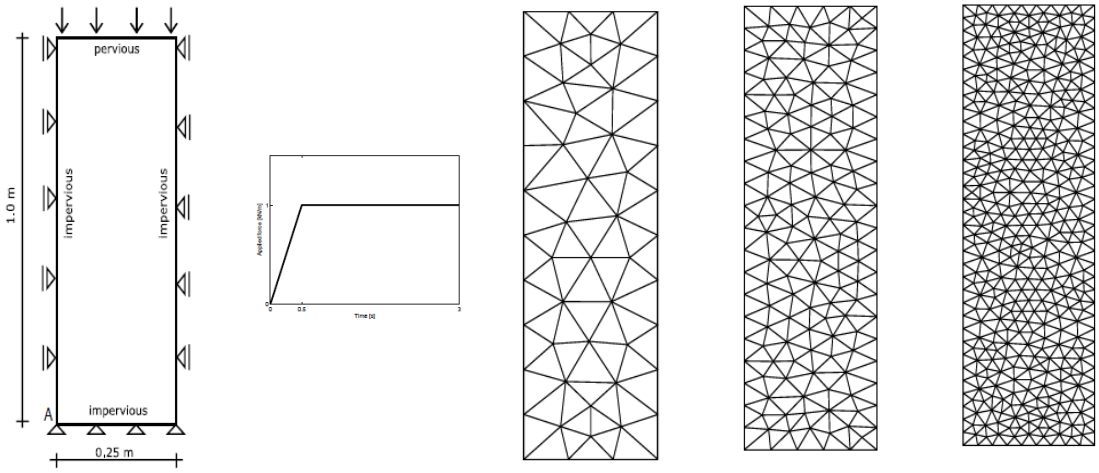

(a) (b) (c) (d) (e)

Fig. 2 Discretization of the sample (a) loading and boundary conditions (b) loading program (c) coarse mesh

We monitor the time evolution of the excess pore pressures in point A and compare the results obtained on the discrete beam lattice model against the results obtained on the continuum model (Smith and Griffiths 2004). Results obtained on the discrete lattice model suggest that the discrete model slightly predicts slightly higher value of excess pore pressures in comparison with the continuum model (Fig. 3(a)). In order to match the results of the continuum model, the value of the coefficient of permeability is increased by 15%. To investigate possible mesh dependency, we repeat the computation for three types of meshes shown in Fig. 2(c)-2(e). From the results, shown in Fig. 3(b), we can conclude that no mesh dependency is observed.

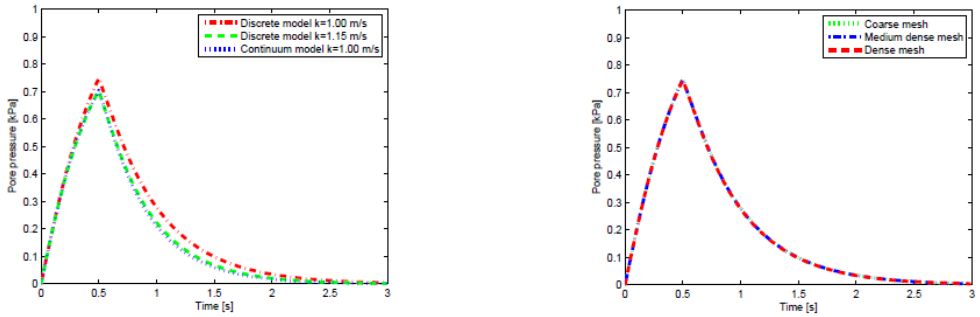

(a) (b)

Fig. 3 Comparison of excess pore pressures (a) continuum-discrete model (b) discrete model with different mesh grading

We repeat the computation with the ramp loading reaching its maximum value at $t = 1$ *s*. From the results, shown in Fig. 4(a), we can conclude that the maximum value of excess pore pressure is, as expected, greater in the case of higher loading rate. Namely, this observation is in accordance

with Terzaghi's principle of effective stresses. In the case of undrained conditions, where water is prevented from draining, the total applied force will be carried by the water in the pores, because the water is assumed to be much stiffer than the soil skeleton. If the water is allowed to drain, then the part of the force will be carried by the soil skeleton and part by the water in the pores. In the case of higher loading rate, the water has less time for draining, and thus the maximum value of excess pore pressure is greater than in the case of lower loading rate. The computed vertical displacements of the top base of the sample are shown in Fig. 4(b). The consolidation represents the time change in the volume of the sample due to the change in the effective stresses. After the excess pore pressure drops to zero, there is no more change in effective stress and we can state that the consolidation process has ended. From Fig. 4(b), we can see that as the value of excess pore pressure approaches zero, the value of vertical displacement approaches constant value marking the end of the consolidation.

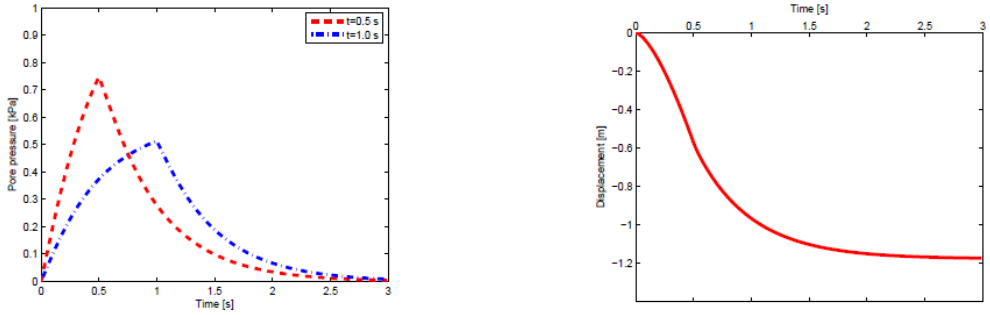

(a) (b)

Fig. 4 Discrete lattice model (a) excess pore pressures (b) vertical displacement of the top of the sample

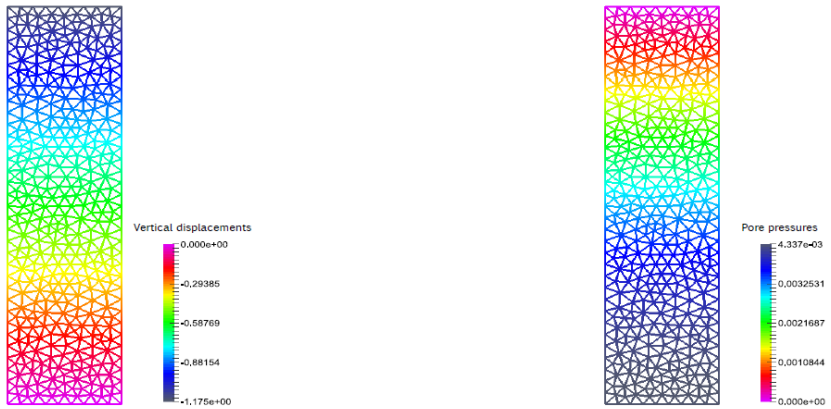

(a) (b)

Fig. 5 Discrete lattice model (a) vertical displacements (b) excess pore pressures

3.2 Plain strain compression test

In this section we simulate a plain strain compression test on a sample of fully saturated over-consolidated clay. The geometry of the specimen and boundary conditions are shown in Fig. 6(a).

The mechanical properties of the Timoshenko beam finite element are shown in Tables 2 and 3. To take into account material heterogeneities, ultimate values of stresses are randomly assigned to every finite element using Gaussian random distribution defined with mean μ and standard deviation σ. The ultimate shear stress for each Timoshenko beam finite element is defined with Mohr-Coulomb law

$$\tau = c + \sigma' \cdot \tan\phi \tag{33}$$

where c is the cohesion, and ϕ is the internal angle of friction of material.

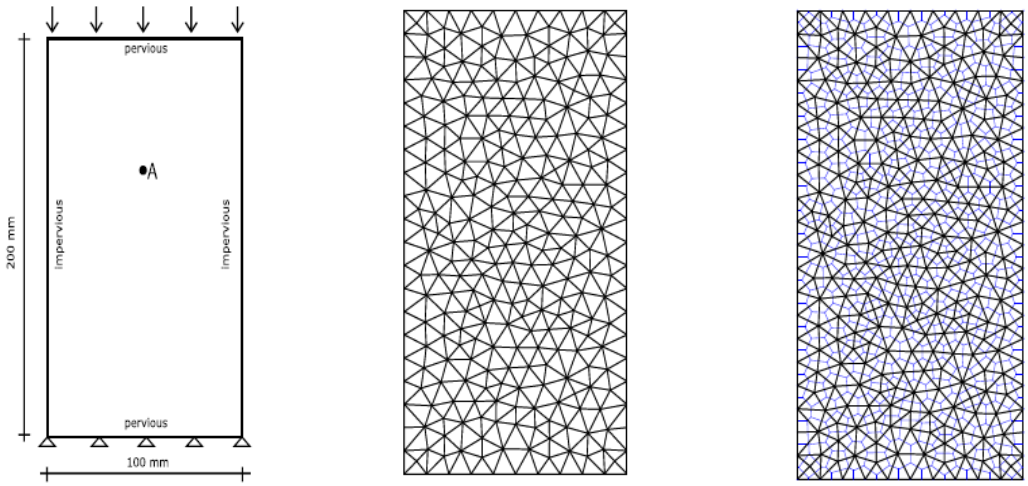

(a) (b) (c)

Fig. 6 Discretization of the specimen (a) loading and boundary conditions (b) mesh (c) Voronoi diagram

Table 2 Mechanical properties of the Timoshenko beam finite element

Young's modulus (kPa)	Poisson's ratio	Yield limit (kPa)	Hardening modulus (kPa)	Fracture limit (kPa)	Fracture energy (N/mm)
$E = 20000$	$v = 0.2$	$\sigma_{y,t} = 10$	$K_t = 2000$	$\mu_t = 12$ $\sigma_t = 1$	$G_{f,t} = 20$
		$\sigma_{y,c} = 100$	$K_c = 2000$	$\mu_c = 120$ $\sigma_c = 10$	$G_{f,c} = 100$
		$\sigma_{y,s} = 12$	$K_s = 2000$	$\mu_s = 15$ $\sigma_s = 1$	$G_{f,s} = 100$

Table 3 Mechanical properties of the Timoshenko beam finite element

Internal angle of friction (°)	Biot coefficient	Biot modulus (kPa)	Coefficient of permeability (m/s)	Unit weight of water (kN/m^3)
$\phi = 11$	$b = 1$	$M \to \infty$	$k = 1 \cdot 10^{-7}$	$\gamma_w = 10$

Our goal is to capture the post-peak response and the failure mechanism in a sample of clay fully saturated with water. For this reason, the test is preformed with vertical displacements

imposed on the top base of the specimen with a constant rate. To investigate the coupling effects, vertical displacements are imposed with two different rates: $v = 1 \cdot 10^{-6}$ m/s and $v = 8 \cdot 10^{-6}$ m/s. The macroscale responses of the sample upon reaching the ultimate load value for different displacement rates do not differ significantly despite different values of generated excess pore pressures (Fig. 7(a)). After intial contraction, the sample begins to exibit dilatant behavior. The dilatant behavior leads to the decrease in the value of excess pore pressures and the evolution of the negative excess pore pressures as shown in Fig. 7(b). Significant coupling effects are observed in the post-peak part of the response. After the compressive strength is reached, the stiffness of the sample decreases. The higher displacement rate in combination with a more deformable sample leads to a greater increase in the values of excess pore pressures than in the case of the lower displacement rate (see Eq. (26)). In the end, this results in a greater value of total vertical reaction. At the end of the loading program, a macrocrack is formed (Fig. 8(c)) leading to the complete failure of the sample.

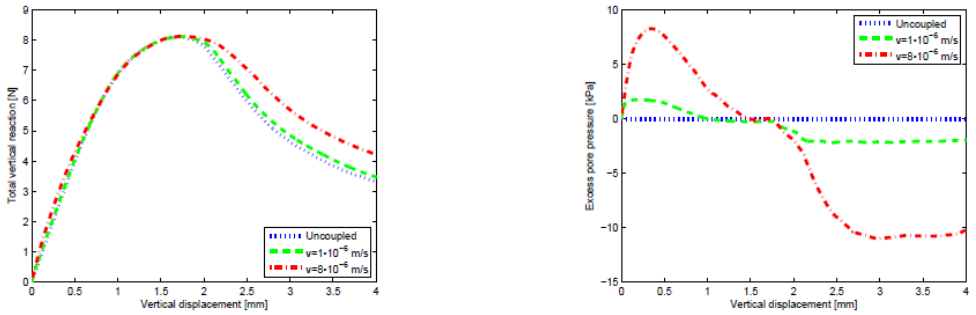

(a) (b)

Fig. 7 Compression test (a) total vertical reaction (b) excess pore pressures ($k = 1 \cdot 10^{-7}$ m/s)

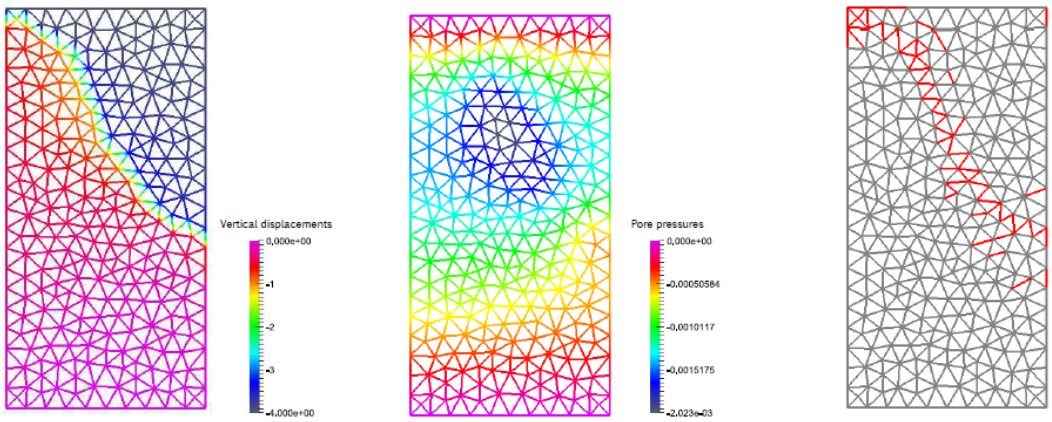

(a) (b) (c)

Fig. 8 Compression test (a) vertical displacements (b) excess pore pressures (c) elements with increasing damage ($k = 1 \cdot 10^{-7}$ m/s, $v = 1 \cdot 10^{-6}$ m/s)

We also preform the computation for two different values of coefficient of permeability:

$k = 1 \cdot 10^{-7}$ m/s and $k = 1 \cdot 10^{-8}$ m/s. The computed responses are shown in Fig. 9(a) and 9(b). We arrive to the same conclusion as in the case of different displacement rates. In the case of lower value of the coefficient of permeability, water takes more time to drain. This results in the generation of the higher values of negative excess pore pressures and in increase in value of total vertical reaction in the post-peak part of the response.

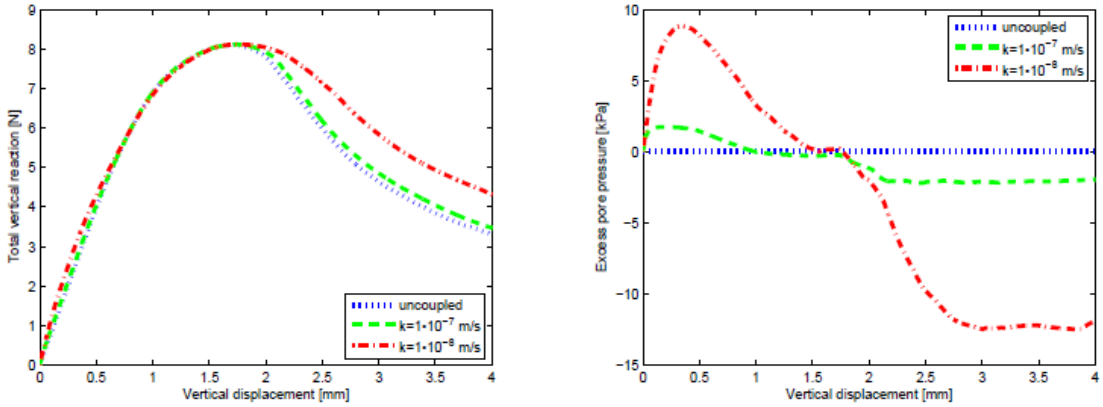

(a) (b)

Fig. 9 Compression test (a) total vertical reaction (b) excess pore pressures ($v = 1 \cdot 10^{-6}$ m/s)

3.3 Coupled soil-foundation system

In this section, we simulate the response of a rigid footing on saturated soil stratum. The geometry and boundary conditions are shown in Fig. 10. The mesh and Voronoi discretization are shown in Fig. 11(a) and 11(b). The mechanical properties of the Timoshenko beam finite element used in numerical simulation are shown in Tables 4 and 5.

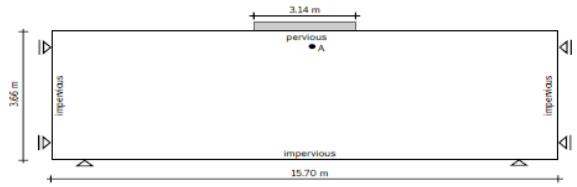

Fig. 10 Configuration of the problem, loading and boundary conditions

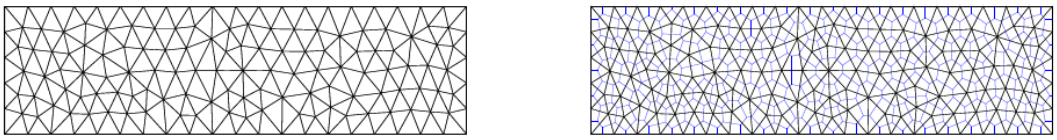

(a) (b)

Fig. 11 Discretization of the specimen (a) mesh (b) Voronoi diagram

Table 4 Mechanical properties of the Timoshenko beam finite element

Young's modulus (MPa)	Poisson's ratio	Yield limit (MPa)	Hardening modulus (MPa)	Fracture limit (MPa)	Fracture energy (MN/m)
$E=160$	$v=0.3$	$\sigma_{y,t}=0.03$	$K_t=60$	$\sigma_{u,t}=0.09$	$G_{f,t}=0.0006$
		$\sigma_{y,c}=0.30$	$K_c=60$	$\sigma_{u,c}=0.90$	$G_{f,c}=0.06$
		$\sigma_{y,s}=0.07$	$K_s=60$	$\sigma_{u,s}=0.13$	$G_{f,s}=0.02$

Table 5 Mechanical properties of the Timoshenko beam finite element

Internal angle of friction (°)	Biot coefficient	Biot modulus (kPa)	Coefficient of permeability (m/s)	Unit weight of water (kN/m^3)
$\phi=17$	$b=1$	$M\rightarrow\infty$	$k=1\cdot10^{-6}$	$\gamma_w=10$

We simulate the response of the rigid footing by imposing uniform vertical displacements with a constant rate along the length of the footing. In order to investigate the coupling effects, we perform the computation for two different displacements rates: $v=2\cdot10^{-5}$ m/s and $v=5\cdot10^{-5}$ m/s. We can conclude that the macroscale response prior to reaching the ultimate load value is significantly influenced by the coupling effects (Fig. 12(a)). The soil under the footing exhibits contractive behaviour as shown in the computed excess pore pressures at point A (Fig. 12(b)). Higher displacement rate causes the generation of higher values of excess pore pressures, which leads to an increase in the value of total vertical reaction. However, for higher rate, the softening part of the response begins at the smaller value of vertical displacement. In the post-peak part of the response, due to water drainage, computed responses for different displacement rates approach the uncoupled response. The shape of the macrocrack formed under the footing, shown in Fig. 14, conicides with the commonly observed shape of the failure wedge.

(a) (b)

Fig. 12 Coupled soil-foundation system (a) total vertical reaction (b) excess pore pressures ($k=1\cdot10^{-6}$ m/s)

(a) (b)

Fig. 13 Coupled soil-foundation system (a) vertical displacements (b) excess pore pressures ($k=1\cdot10^{-6}$ m/s, $v=2\cdot10^{-5}$ m/s)

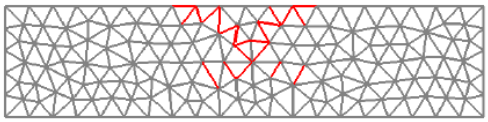

Fig. 14 Elements with increasing damage ($k = 1 \cdot 10^{-6}$ m/s, $v = 2 \cdot 10^{-5}$ m/s)

We repeat the computation for two different values of coefficient of permeability: $k = 1 \cdot 10^{-5}$ m/s and $k = 1 \cdot 10^{-6}$ m/s. For the higher value of coefficient of permeability, the computed macroscale response approaches the uncoupled response (Fig. 15(a)). A higher coefficient of permeability means that the soil is more permeable and that water is able to drain faster. This leads to the generation of lower values of excess pore pressures (Fig. 15(b)) and a decrease in the value of total reaction compared to the less permeable soil.

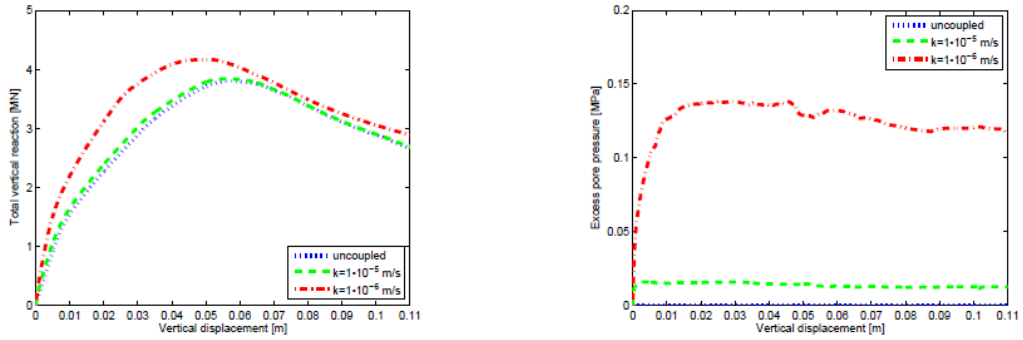

(a) (b)

Fig. 15 Coupled soil-foundation systems (a) total vertical reaction (b) excess pore pressures ($v = 5 \cdot 10^{-5}$ m/s)

4. Conclusions

In this paper, we used a discrete beam lattice model to simulate the response of the fully saturated soil subjected to external loading. The behavior and failure mechanism in the saturated soil are captured on the mesh of inelastic Timoshenko beam finite elements. With the aim of representing the crack formation in modes I and II, Timoshenko beam finite elements are enriched with additional kinematics in terms of strong discontinuities in axial and transverse direction. The coupling between the solid and the fluid phase is introduced through Biot's porous media theory.

The numerical simulation of localized failure in saturated soil is preformed by imposing vertical displacements with different rates in order to investigate the effects of coupling the soil and the pore fluid on the computed response. We have concluded that the model is able to capture the true failure mechanism in the saturated soil and to accurately predict the time evolution of excess pore pressures in the cases where soil exhibits dilatant or contractive behavior. The discrete beam lattice model used in this paper, ensures the efficient numerical preformance in terms of computational time and rate of convergence. The predictive value of the model can be ensured if the failure parameters of the Timoshenko beam finite elements are identified by using parameter identification methods against some of the standard tests, as shown in this work.

Acknowledgments

This work was supported by the French Ministry of Foreign Affairs and French Embassy in Bosnia and Herzegovina. Professor Adnan Ibrahimbegovic was supported by funding for Chaire de Mécanique Picardie (120-2015 RDISTRUCT-000010 and RDISTRUCT-000010) and EU funding (FEDER). This support is gratefully acknowledged.

References

Armero, F. and Callari, C. (1999), "An analysis of strong discontinuities in a saturated poro-plastic solid", *J. Numer. Meth. Eng*., **1999**(46), 1673-1698.

Benkemoun, N., Hautefeuille, M., Colliat, J.B. and Ibrahimbegovic, A. (2010), "Failure of heterogeneous materials: 3D meso-scale FE models with embedded discontinuities", *J. Numer. Meth. Eng*., **2010**(82), 1671-1688.

Benkemoun, N., Ibrahimbegovic A. and Colliat J.B. (2010), "Anisotropic constitutive model of plasticity capable of accounting for details of meso-structure of two-phase composite material", *Comput. Struct*., **2012**(90), 153-162.

Biot, M.A. (1941), "General theory of three-dimensional consolidation", *J. Appl. Phys*., **1941**(12), 155-164.

Bolander, J.E. and Berton., S. (2004), "Simulation of shrinkage induced cracking in cement composite overlays", *Cement Concrete Compos*., **2004**(26), 861-871.

Callari, C. and Armero, F. (2002), "Finite element methods for the analysis of strong discontinuities in coupled poro-plastic media", *Comput. Meth. Appl. Mech. Eng*., **2002**(191), 4371-4400.

Callari, C. and Armero, F. (2004), "Analysis and numerical simulation of strong discontinuities in finite strain poroplasticity", *Comput. Meth. Appl. Mech. Eng*., **2004**(193), 2941-2986.

Callari, C., Armero, F. and Abati, A. (2010), "Strong discontinuities in partially saturated poroplastic solids", *Comput. Meth. Appl. Mech. Eng*., **2010**(199)(23), 1513-1535.

De Borst, R., Réthoré, J. and Abellan, M.A. (2006), "A numerical approach for arbitrary cracks in a fluid-saturated medium", *Arch. Appl. Mech*., **2006**(75), 595-606.

Do, X.N., Ibrahimbegovic, A. and Brancherie, D. (2015), "Combined hardening and localized failure with softening plasticity in dynamics", *Coupled Syst. Mech*., **2015**(4), 115-136.

Geuzaine, C. and Remache, J.F. (2009), "Gmsh: A 3-D finite element mesh generator with built-in pre- and post-processing facilities", *J. Numer. Meth. Eng*., **2009**(79), 1309-1331.

Grassl, P. (2009), "A lattice approach to model flow in cracked concrete", *Cement Concrete Compos*., **2009**(31), 454-460.

Hadzalic E., Ibrahimbegovic, A. and Dolarevic, S. (2017), "Failure mechanisms in coupled soil-foundation systems", *Coupled Syst. Mech*., **2017**(6), 110-136

Ibrahimbegovic, A. (2009), *Nonlinear Solid Mechanics: Theoretical Formulations and Finite Element Solution Methods*, Springer.

Ibrahimbegovic, A. and Delaplace, A. (2003), "Microscale and mesoscale discrete models for dynamic fracture of structures built of brittle material", *Comput. Struct*., **2003**(81), 1255-1265.

Imamovic, I., Ibrahimbegovic, A., Knopf-Lenoir, C. and Mesic, E. (2015), "Plasticity-damage model parameters identification for structural connections", *Coupled Syst. Mech*., **2015**(4), 337-364.

Larsson, J. and Larsson, R. (2000), "Finite-element analysis of localization of deformation and fluid pressure in an elastoplastic porous medium", *J. Sol. Struct*., **2000**(37), 7231-7257.

Lewis, R.W. and Schrefler, B.A. (1998), *The Finite Element Method in the Static and Dynamic Deformation and Consolidation of Porous Media*, John Wiley and Sons.

Nikolic, M. and Ibrahimbegovic, A. (2015), "Rock mechanics model capable of representing initial heterogeneities and full set of 3D failure mechanisms", *Comput Meth. Appl. Mech. Eng*., **2015**(290), 209-227.

Nikolic, M., Ibrahimbegovic, A. and Miscevic, P. (2015), "Brittle and ductile failure of rocks: Embedded discontinuity approach for representing mode I and mode II failure mechanisms", *J. Numer. Meth. Eng.*, **2015**(102), 1507-1526.

Nikolic, M., Ibrahimbegovic, A. and Miscevic, P. (2016), "Discrete element model for the analysis of fluid-saturated fractured poro-plastic medium based on sharp crack representation with embedded strong discontinuities", *Comput. Meth. Appl. Mech. Eng.*, **2016**(298), 407-427.

Nikolic, M., Karavelic, E., Ibrahimbegovic, A. and Miscevic, P. (2017), "Lattice element models and their peculiarities", *Arch. Comput. Meth. Eng.*

Prevost, J.H. (1983), "Implicit-explicit schemes for nonlinear consolidation", *Comput. Meth. Appl. Mech. Eng.*, **1983**(39), 225-239.

Réthoré., J., De Borst, R. and Abellan, MA. (2008), "A two-scale model for fluid flow in an unsaturated porous medium with cohesive cracks", *Comput. Mech.*, **2008**(42), 227-238.

Šavija, B., Lukovic, M. and Schlangen, E. (2014), "Lattice modeling of rapid chloride migration in concrete", *Cement Concrete Compos.*, **2014**(61), 49-63.

Šavija, B., Pacheco J.A. and Schlangen, E. (2013), "Lattice modeling of chloride diffusion in sound and cracked concrete", *Cement Concrete Compos.*, **2013**(42), 30-40.

Secchi., S. and Schrefler, B.A. (2014), "Hydraulic fracturing and its peculiarities", *Asia Pac. J. Comput. Eng.*, **2014**(1), 1-8.

Singh, M. and Sawant, V.A. (2014), "Parametric study on flexible footing resting on partially saturated soil", *Coupled Syst. Mech.*, **2014**(3), 233-245.

Smith, M. and Griffiths, D.V. (2004), *Programming the Finite Element Method*, 4th Edition, John Wiley & Sons.

Terzaghi, K. (1943), *Theoretical Soil Mechanics*, Wiley.

Zienkiewicz, O.C. and Shiomi, T. (1984), "Dynamic behavior of saturated porous media; the generalized biot formulation and its numerical solution", *J. Numer. Analy. Meth. Geomech.*, **1984**(8), 71-96.

Zienkiewicz, O.C. and Taylor, R.L. (2005), *The Finite Element Method, Vols. I, II, III*, Elsevier.

AI